DESIGN AND ANALYSIS OF CONTROLLERS FOR BOOST CONVERTER USING LINEAR AND NONLINEAR APPROACHES

A Thesis
Submitted to
the Temple University Graduate Board

In Partial Fulfillment
of the Requirements for the Degree
MASTER OF SCIENCE IN ELECTRICAL ENGINEERING

---

by
Youqi Guo
August 2018

Thesis Approvals:

Dr. Saroj Biswas, Thesis Advisor, Electrical and Computer Engineering
Dr. Qing Dong, Naval Warfare Surface Center, Philadelphia
Dr. Liang Du, Electrical and Computer Engineering

ABSTRACT

Power converters are electronic circuits for conversion, control and regulation of electric power for various applications, such as from tablet computers in milliwatts to electric power systems at megawatts range. There are three basic types of power converters: buck (output voltage less than the input voltage), boost (output voltage higher than the input voltage) and buck-boost converters. The reliability of the power converters has become an essential focus of industrial applications. This research presents modeling and control of DC/DC boost converter using several control methods, such as Proportional-Integral (PI), Linear Quadratic Regulator (LQR) control, and nonlinear control concepts. Based on standard circuit laws, a mathematical model of the boost converter is derived which is expressed as a bilinear system. First a small signal model of the converter is derived to analyze the small deviations around the steady-state operating point which is used to develop closed loop control using the PI and the LQR methods. Simulation results show that the performance of the converter is good for operation around the operating state, however is unacceptable if there are large variations in the load or the reference input. To improve the performance of the closed loop system, the nonlinear control concept is used which shows excellent closed loop performance under large variations of load or setpoint. Comparative simulation results are presented for closed loop performance under various types of disturbances including random variations in load.

ACKNOWLEDGEMENTS

I would first like to thank my advisor Dr. Saroj Biswas and my committee members Dr. Qing Dong and Dr. Liang Du. The work would not be finished without their guidance, patience and constant encouragement. I must also express my gratitude to my parents and girlfriend for their loving support.

TABLE OF CONTENTS

LIST OF FIGURES

LIST OF TABLES

CHAPTER 1

INTRODUCTION

This thesis is concerned with the modeling and control of DC/DC boost converter. In this chapter, research motivation and objectives are presented. The organization of this thesis is given at the end of this chapter.

1.1 Motivation

Power converters are electronic circuits related to conversion, control and regulation of electric power. The power range can be from milliwatts in tablet computer, up to megawatts, for example, in electric power systems. Since the first power electronic devices invented in 1900s, especially with the development of semiconductor technology, a number of topologies for buck, boost and buck-boost converters were designed, developed and analyzed in detail [1]. The reliability of the power converters has become an essential focus of industrial applications. To achieve a long useful life, electronic devices and its control circuit have to be extremely robust [2, 3]. The total efficiency is a main concern of the power electronic circuits. Firstly, high efficiency means more saving energy which directly gives the financial benefit. Even a minor efficiency improvement in converter circuits leads to visible profitability of investment in the electronic market. Secondly, the reduced cost of energy translates to less generation which mitigates environmental pollution indirectly [4]. Another emphasis is disturbance

rejection. For instance, load variations in power systems are common due to temporary short circuits along transmission lines, additional sources of friction that appear momentarily in generators and motors [5]. Because of various work conditions and output requirements, different types of controllers are necessary to be investigated and applied. Our goal of this research is to model a boost converter, design different controllers and evaluate them under various load disturbance and reference variation to verify its stability.

1.2 Research Objectives

As was said before, this thesis focuses on modeling and control of DC-DC boost converter. As is well known, in different work condition, power converters have different properties and applications, and hence they may have different control objectives. For example, in power grid, they have to operate under changing demands, variable load pulse, and even nonlinear loads, with electricity provided by generators and transmission equipment which are not perfectly reliable [6]. As a result of load variations and unstable conditions, implementation of appropriate feedback control becomes general method to maintain voltage regulation. With development of control theory, many control methods have been investigated and implemented on power converters with different objectives and operations. In this thesis, two linear control methods and one nonlinear control algorithm are investigated and compared for a boost converter. The control goal is to ensure the output voltage tracks to a desired value in the presence of various disturbances, such as load variations and reference input variations.

1.3 Outline of the Proposal

Chapter 2 presents the fundamental concepts of the boost converter and develops a complete mathematical model which is used in this thesis. Two linear control methods, PI control and LQR control, are derived and evaluated in Chapter 3 and Chapter 4, respectively. Chapter 5 presents the application of nonlinear control method along with simulation results which is followed by conclusions and future work in Chapter 6.

CHAPTER 2

BACKGROUND

This chapter presents the fundamental concepts of various types of power converters used in industry. Also we derive a mathematical model of the boost converter based on circuit theories. A linear model of the boost converter is also developed to facilitate the design of controllers.

2.1 Converters Classification

As mentioned above, power converters control the flow of power between the output and input by transforming the voltage or current into what is desired for an application. Based on the different type of conversion made between output and input, the most generic classification of power conversion system is [7]:

- DC to DC converter
- DC to AC inverter
- AC to DC rectifier
- AC to AC transformer

2.1.1 DC to DC Converters

DC-DC converters are used to convert DC power input to another DC level. They can be classified as two categories: isolated and non-isolated. The main difference between these two types is whether the circuit has direct DC connection between input and output [8]. The isolated DC-DC converter has transformer to connect input and output which can filter noise and operate in high efficiency while is more complicated than non-isolated converters. Non-isolated DC-DC converter includes six classical topologies: buck converter, boost converter, buck/boost converter, Cuk converter, zeta converter and sepic converter. There are four popular types of isolated DC-DC converters: flyback converter, forward converter, single-ended two-transistor forward converter and phase shift full-bridge converter [9]. DC/DC converters are widely employed in low-power circuits such as cell phones and laptop computers which are powered primarily by batteries. These kind of devices usually contain some sub-circuits which regulate output voltage from batteries or external supply to a required level.

2.1.2 DC to AC Inverters

DC-AC inverters are used to generate a sinusoidal ac output such as in uninterruptible AC power supplies and AC motor drives [10]. These kind of devices can be controlled in both magnitude and frequency. However, due to the system structure, an efficient control is quite complicated. Usually, all practical devices which contain DC-AC inverter is composed of multiple stages, and a cascaded controller is employed to control the multiple input DC-DC converter and DC-AC inverters simultaneously.

2.1.3 AC to DC Rectifier

AC-DC rectifiers, or also called AC-DC converters, can convert AC voltage provided by electric utility, for example, to a desired DC voltage. In most power electronic applications, the first step is converting the power input which is in the form of a sine wave AC voltage to a appropriate DC voltage. The circuits are formed by uncontrolled diode, silicon-controlled thyristor or controlled IGBT rectifiers. Selection of rectifiers depend on the practical cost, ripple requirement, current distortion allowed and so on. The main application of rectifiers are DC power supply, DC servo drives etc.

2.1.4 AC to AC Transformer

AC-AC transformers are employed to convert the input AC voltage to a different amplitude of output AC voltage. The efficiency of transformers is mainly dependent on core losses or iron losses and copper loss. By using transformer, the power conversion efficiency of DC-DC boost convert connected to AC grid can be improved [11].

2.2 Switched-mode Power Converters

Among all electronic converters devices, the switched-mode power converters (SMPC) is the most common technology [12]. They provide DC loads with a regulated output voltage by converting an input voltage signal. Power is controlled by electronic switches that are periodically switched "on" and "off" at high frequency. Hence, the low switching losses and low conduction losses ensure high efficiency and power density that the linear mode device does not

have. So even if a filter is required to reduce output voltage ripple and LC components lead to non-negligible EMC emissions, these SMPC devices become to the most ubiquitous converters [13].

2.3 Boost Converter

The boost converter is used to step-up an input DC voltage to some higher DC level. So it is also called as step up converter. This section presents working principle of boost converter based on a basic topology and its some applications.

2.3.1 Basic Concept

Fig. 2.1 shows the basic circuit of a boost converter. The boost converter circuit includes a switching transistor, together with the inductor L, capacitor C and diode D. In this example, a MOSFET is selected as switch device. It is noting that bipolar power transistors and IGBT can also be used in power switching based on the choice of the current, voltage, switching speed and cost considerations [14].

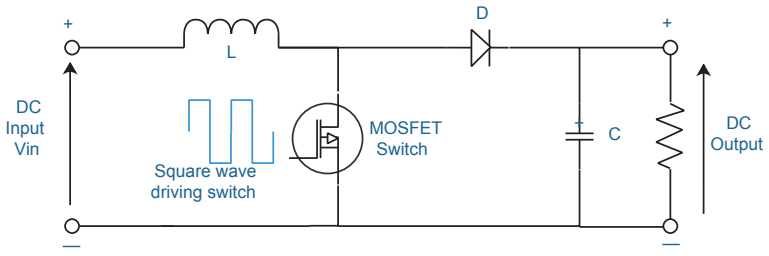

Figure 2.1: Basic Boost Converter

The key working principle of boost converter is that the tendency of inductor to resist sudden current changes by varying magnetic field [15]. When switch

is on, the energy stored in inductor is in the form of magnetic energy and it is discharged to load while switch is off. The capacitor is always designed large enough to ensure constant and smooth output stage.

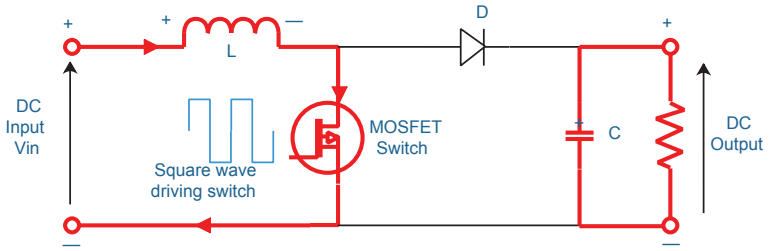

Figure 2.2: Boost Converter Operation at Switch ON

Fig. 2.2 shows the circuit path during the high voltage level of square wave cycle applied to the switch, which means the MOSFET turns on. During this period, the inductor is charged by input DC power and stores energy by producing magnetic field. Therefore current flows through inductor L from positive to negative terminal. Meanwhile, during this switch ON period, the load is supplied energy by capacitor discharging.

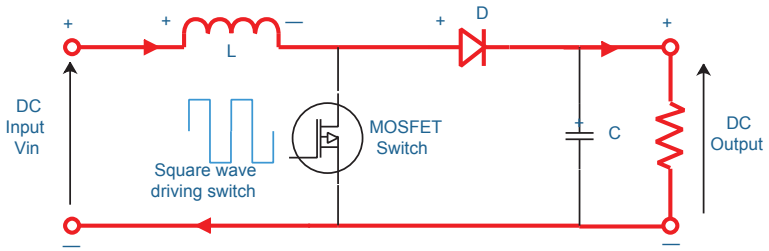

Figure 2.3: Boost Converter Operation at Switch OFF

Fig. 2.3 illustrates the circuit action during the low level of switching square wave, which means the MOSFET turns OFF. The magnetic field created during switch on is destroyed to keep current still flowing from left to right side. As a result, two sources, inductor and input DC power, supply energy to the load causing a higher voltage and charging capacitor C.

With a steady state duty cycle D, the switching function is shown in Fig. 2.4. The inductor voltage V_L pulsates between two values: V_{in} and $-(V_o - V_{in})$ as plotted in Fig. 2.4. Since the average inductor voltage is zero, the volt-second areas during the two sub-intervals are equal in magnitude and opposite in sign.

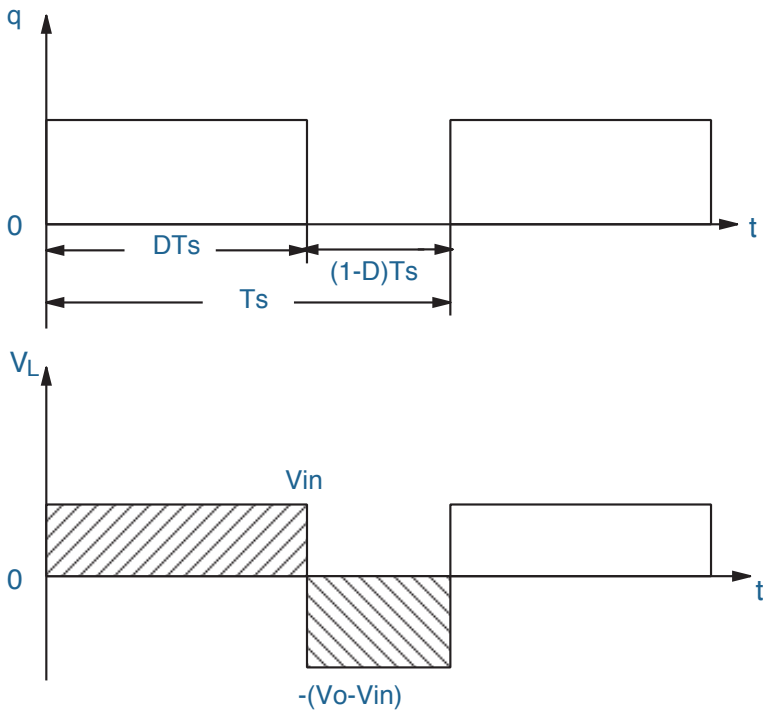

Figure 2.4: Boost Converter Waveforms

The input/output voltage ratio can be obtained using the inductor voltage waveform whose average is zero in dc steady state [10]. This gives

$$V_{in}(DT_s) = (V_o - V_{in})(1 - D)T_s \tag{2.1}$$

Hence,

$$\frac{V_o}{V_{in}} = \frac{1}{1 - D} \tag{2.2}$$

2.3.2 Applications

Switched mode boost converter can be used for many purposes. Since it was invented for hundred year, it is wildly applied to not only traditional industries such as electric power system but also emerging industries like electric viehcle [16]. For example, the motors used in driving electric automobiles require high voltages, in the range of 500V, than could be supplied by solo battery. Even a bunch of battery pack are used, it is too heavy and large to be practical. As a solution, fewer batteries and proper boost converter which is able to boost the DC voltage of battery to required voltage level [17]. The DC input to a boost converter can be obtained from many sources, such as batteries, rectified AC from the mains supply, or DC from solar panels, fuel cells, dynamos, and DC generators, etc.

In recent years, boost converters have also drawn new interest in renewable energy applications, especially in wind and solar power generation. Using a boost converter with proper control algorithm, Dual-stator Winding Induction Generator (DWIG) can produce higher DC voltage operating at Maximum Power Point Tracking (MPPT) at low speed and low voltage condition [18]. Boost converters are also used for MPPT tracking in solar power generation.

2.4 System Modeling

In this section, we derive a mathematical model of the boost converter which will be used for controller design and analysis of performance. Derivation of the circuit model is based on standard circuit theories, such as Kirchhoff's voltage and current laws.

State-space averaging method is a very common method used to analyze and design controller and power electronics circuit which is based on linear RLC elements, independent power and the network consisting of switch. The voltage of capacitor and the current of inductor are used as state variables. The basic circuit concepts are used to write circuit equations according to the power switchings of ON and OFF states. Since the switching occurs at very high frequencies, it is appropriate to find an average model of the circuit corresponding to the ON and the OFF states. This leads to the bilinear model of the boost converter for the state space average model.

2.4.1 Averaging Method

In a DC-DC boost converter circuit, the system actually works in two modes: switch open mode and switch close mode. In state space description, the state equations of two modes can be described as following:

$$\begin{aligned} \dot{x} &= A_1 x + B_1 u \quad 0 \leq t \leq dT, \quad \text{Switch ON} \\ \dot{x} &= A_2 x + B_2 u \quad dT \leq t \leq T, \quad \text{Switch OFF} \end{aligned} \tag{2.3}$$

where d is the duty cycle in one T period, which is a positive number, $0 \leq d \leq 1$. Then the average state space model is:

$$\dot{x} = \bar{A}x + \bar{B}u \tag{2.4}$$

where

$$\begin{aligned} \bar{A} &= A_1 d + A_2(1-d) \\ \bar{B} &= B_1 d + B_2(1-d) \end{aligned} \tag{2.5}$$

A simple proof is shown blow. We assume the capacitor voltage and inductor current change linearly in each working mode, ON or OFF. This is justifiable since the converter switching occur at very high frequencies. Then for the switch ON period, we have

$$\begin{aligned} \int_0^{dT} \dot{x}\mathrm{d}t &= \int_0^{dT} (A_1 x + B_1 u)\mathrm{d}t \\ x(dT) - x(0) &\simeq (A_1 x + B_1 u)dT \end{aligned} \tag{2.6}$$

Similarly, for the OFF period, we have

$$\begin{aligned} \int_{dT}^{T} \dot{x}\mathrm{d}t &= \int_{dT}^{T} (A_2 x + B_2 u)\mathrm{d}t \\ x(T) - x(dT) &\simeq (A_2 x + B_2 u)(T - dT) \end{aligned} \tag{2.7}$$

Combining equations (2.6) and (2.7):

$$\begin{aligned} &x(T) - x(0) = (A_1 x + B_1 u)dT + (A_2 x + B_2 u)(1-d)T \\ &\implies \dot{x} = \frac{x(T) - x(0)}{T} = (A_1 d + A_2(1-d))x + (B_1 d + B_2(1-d))u \end{aligned} \tag{2.8}$$

which gives the state space average model as equations (2.4) and (2.5).

2.4.2 Boost Converter State Space Average Model

An accurate model is essential to design controllers. In this section, averaging method is used to approximate the system behavior [19] as discussed in the previous section.

Fig. 2.5 shows the accurate model of a boost converter which includes a series of parasitic parameters. R_L, V_D, R_C are parasitic resistor of inductor, forward voltage drop of diode, and equivalent series resistor (ESR) of capacitor, respectively.

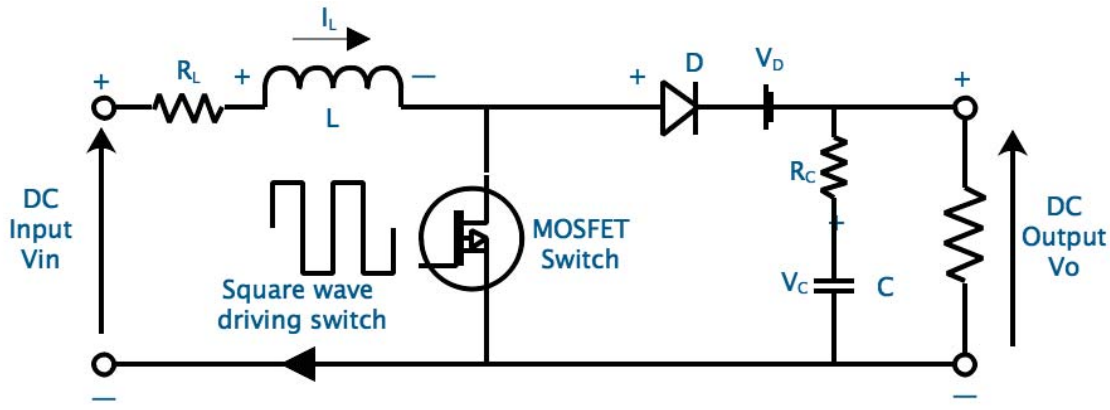

Figure 2.5: The Accurate Model of Boost Converter

- When the switch is closed, the battery circuit is closed through the switch, and at the same time the capacitor discharges through the load resistance. The capacitor is discharged to supply energy to load:

$$V_0(t) = V_C(t) - \frac{V_0(t)}{R} R_C \rightarrow V_0(t) = \frac{R}{R + R_C} V_C(t) \tag{2.9}$$

Discharged current is $-\frac{V_o(t)}{R}$

The state equations are

$$\begin{cases} L\dfrac{dI_L(t)}{dt} = V_{in} - I_L(t)R_L \\ C\dfrac{dV_C(t)}{dt} = -\dfrac{V_C(t)}{R + R_C} \end{cases} \tag{2.10}$$

where I_L denotes the current of inductor, which equals to I_{in}; V_C denotes the voltage of the capacitor. And the output voltage V_O is written by

$$V_O = \frac{R}{R + R_C} V_C \tag{2.11}$$

- When switch is opened, the stored energy in the capacitor discharges through the diode. The charging current of capacitor is $I_L(t) - \frac{V_o(t)}{R}$; this gives the state equations as

$$\begin{cases} L\dfrac{dI_L(t)}{dt} = V_{in} - V_D - (R_L + \dfrac{RR_C}{R + R_C})I_L(t) - \dfrac{R}{R + R_C}V_C(t) \\ C\dfrac{dV_C(t)}{dt} = \dfrac{RR_C}{R + R_C}I_L(t) - \dfrac{V_C(t)}{R + R_C} \end{cases} \tag{2.12}$$

The output V_O is described as:

$$V_O = \frac{R}{R + R_C}(V_C + I_L R_C) \tag{2.13}$$

Denote the state variables as $x_1 = I_L(I_{in})$, $x_2 = V_C$, $y = V_O$ and rewrite equations (2.10) and (2.12) in state space:

- When switch closed

$$\begin{aligned} \begin{bmatrix} \dot{x_1} \\ \dot{x_2} \end{bmatrix} &= \begin{bmatrix} -\frac{R_L}{L} & 0 \\ 0 & -\frac{1}{C(R+R_C)} \end{bmatrix} \begin{bmatrix} x_1 \\ x_2 \end{bmatrix} + \begin{bmatrix} \frac{V_{in}}{L} \\ 0 \end{bmatrix} \\ y &= \begin{bmatrix} 0 & \frac{R}{R+R_C} \end{bmatrix} \begin{bmatrix} x_1 \\ x_2 \end{bmatrix} \end{aligned} \tag{2.14}$$

- When switch opened

$$\begin{aligned} \begin{bmatrix} \dot{x_1} \\ \dot{x_2} \end{bmatrix} &= \begin{bmatrix} -\frac{RR_C+(R+R_C)R_L}{L(R+R_C)} & -\frac{R}{L(R+R_C)} \\ \frac{R}{C(R+R_C)} & -\frac{1}{C(R+R_C)} \end{bmatrix} \begin{bmatrix} x_1 \\ x_2 \end{bmatrix} + \begin{bmatrix} \frac{V_{in}-V_D}{L} \\ 0 \end{bmatrix} \\ y &= \begin{bmatrix} \frac{RR_C}{R+R_C} & \frac{R}{R+R_C} \end{bmatrix} \begin{bmatrix} x_1 \\ x_2 \end{bmatrix} \end{aligned} \tag{2.15}$$

The state space average model is then obtained by averaging the state space matrices of two different working modes using the average method mentioned in Section 2.4.1. The average model is shown as:

$$\begin{bmatrix} \dot{x_1} \\ \dot{x_2} \end{bmatrix} = \begin{bmatrix} -\frac{RR_C}{L(R+R_C)}(1-d) - \frac{R_L}{L} & -\frac{R}{L(R+R_C)}(1-d) \\ \frac{R}{C(R+R_C)}(1-d) & -\frac{1}{C(R+R_C)} \end{bmatrix} \begin{bmatrix} x_1 \\ x_2 \end{bmatrix} + \begin{bmatrix} -\frac{V_D}{L}(1-d) + \frac{V_{in}}{L} \\ 0 \end{bmatrix}$$
$$y = \begin{bmatrix} \frac{RR_C}{R+R_C}(1-d) & \frac{R}{R+R_C} \end{bmatrix} \begin{bmatrix} x_1 \\ x_2 \end{bmatrix} \tag{2.16}$$

The complete model symbolically expressed as $\dot{x} = \bar{A}x + \bar{B}$ and $y = \bar{C}x$ which will be used in the next chapter to design a controller. First we verify accuracy of the state space model.

2.4.3 Parameters Design

This section shows parameter selection of the boost converter modeled above. Input voltage V_{in} and input current I_L are selected as $5V$ and $2.2A$ as nominal working condition, respectively. Nominal output working voltage is chosen as $12V$. Inductance L and capacitance C are calculated as following equations [7]:

$$L > \frac{dV_{in}(1-d)}{2fI_{out}} \tag{2.17}$$

$$C > \frac{I_{out}}{V_{ripple}f} \tag{2.18}$$

Where d is nominal duty cycle selected as 0.58 and V_{ripple} Maximum allowable voltage ripple. I_{out} is output current which can be calculated by input power and load resistance. Table 2.1 presents complete parameters used in this research.

Table 2.1: Design Values of the Boost Converter

No.	Parameters	Design Values
01	Input Voltage, V_{in}	5V
02	Output Voltage, V_o	12V
03	Inductance, L	$9mH$
04	Capacitance, C	$1mF$
05	Load Resistance, R_{load}	13Ω
06	Capacitor Parasitic Resistance, R	0.01Ω
07	Inductor Parasitic Resistance, R_L	0.05Ω
08	Input power, P_{in}	$11W$
09	Switch frequency, f	$50KHz$
10	Nominal duty cycle, d	0.58
11	Maximum allowable voltage ripple, V_{ripple}	0.05

2.4.4 Verification of Average Model

This section presents the simulation results of the open loop response for both the average model and the switching model. The average model is described by equations (2.16) whereas the switching model is given by equations (2.14) and (2.15). In order to confirm average model can represent switch model, comparison between these two models is shown in Fig. 2.6. Nominal duty cycle and input voltage are used for the simulation.

Figure 2.6 shows that both average model (solid wave) and switching model (saw wave) approach to the expected output voltage and inductor current value. Clearly, the average model gives excellent approximation of switch model, which implies the average model works as intended. So this model will be used to design and evaluate controller performance in the rest part of the thesis.

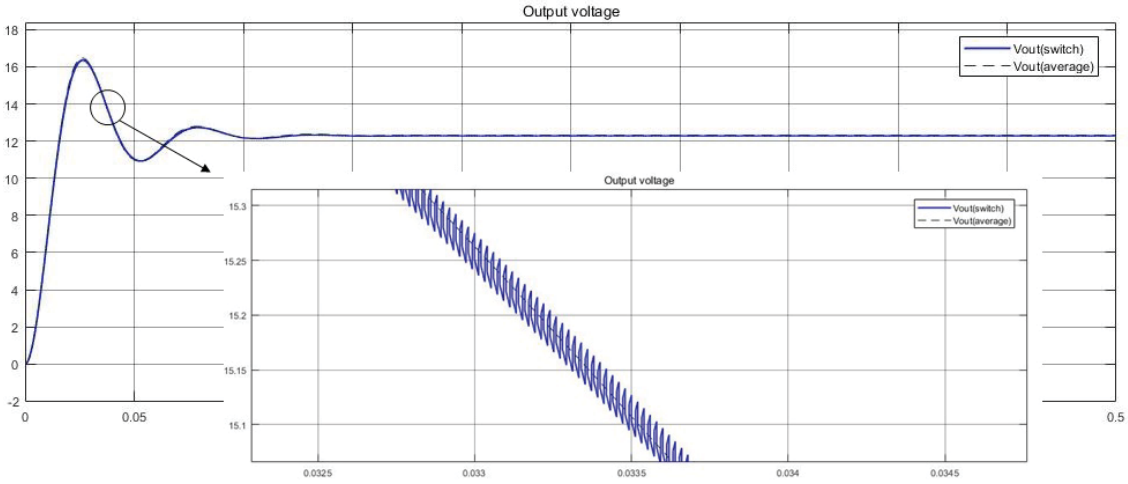

Figure 2.6: Verification of Average Model for Boost Converter

2.5 Average Model Linearization

By observing the average model shown above, it is still a nonlinear model because the duty cycle d, which is the input variable, is just inside the state space matrix. However, to apply PI controller for boost converter using linear controller design method, linearization of the average model is necessary. Euler's method is applied for the linearization process, which is the simplest, where assume a sufficiently small inductor current increment Δx_1, capacitor voltage increment Δx_2 and duty cycle increment Δd. Using these increments in equation (2.16), we have

For x_1:

$$\begin{aligned} \dot{x_1} + \Delta\dot{x_1} = &-\frac{RR_C}{L(R+R_C)}(1-(d+\Delta d)(x_1+\Delta x_1) \\ &-\frac{R}{L(R+R_C)}(1-(d+\Delta d))(x_2+\Delta x_2) - \frac{V_D}{L}(1-(d+\Delta d) \end{aligned} \tag{2.19}$$

For x_2:

$$\begin{aligned}\dot{x_2} + \Delta\dot{x_2} = &-\frac{R}{C(R+R_C)}(1-(d+\Delta d)(x_1+\Delta x_1) \\ &-\frac{1}{C(R+R_C)}(x_2+\Delta x_2)\end{aligned} \tag{2.20}$$

By canceling the equalities and eliminating the second order terms:

$$\begin{aligned}\Delta\dot{x_1} = &(-\frac{RR_C}{L(R+R_C)}(1-d) - \frac{R_L}{L})\Delta x_1 \\ &-\frac{R}{L(R+R_C)}(1-d)\Delta x_2 + (\frac{R(R_C x_1 + x_2)}{L(R+R_C)} + \frac{V_D}{L})\Delta d\end{aligned} \tag{2.21}$$

$$\Delta\dot{x_2} = -\frac{R}{C(R+R_C)}(1-d)\Delta x_1 - \frac{1}{C(R+R_C)}\Delta x_2 - \frac{Rx_1}{C(R+R_C)}\Delta d \tag{2.22}$$

Rewriting the above equations in matrix form, we obtain the linear model of the boost converter shown below:

$$\begin{aligned}\begin{bmatrix}\Delta\dot{x_1} \\ \Delta\dot{x_2}\end{bmatrix} = &\begin{bmatrix}-\frac{RR_C}{L(R+R_C)}(1-d) - \frac{R_L}{L} & -\frac{R}{L(R+R_C)}(1-d) \\ \frac{R}{C(R+R_C)}(1-d) & -\frac{1}{C(R+R_C)}\end{bmatrix}\begin{bmatrix}\Delta x_1 \\ \Delta x_2\end{bmatrix} \\ &+\begin{bmatrix}\frac{R(R_C I_{ss}+V_{ss})}{L(R+R_C)} \\ -\frac{RI_{ss}}{C(R+R_C)}\end{bmatrix}\Delta d\end{aligned} \tag{2.23}$$

where V_{ss} and I_{ss} denote the steady states of V_{out} and I_L, and d is the duty cycle in steady state. Also, the output in equation (2.16) is linearized as,

$$\Delta y = \begin{bmatrix}\frac{RR_C(1-d)}{R+R_C} & \frac{R}{R+R_C}\end{bmatrix}\Delta x + \begin{bmatrix}\frac{RR_C I_{SS}}{R+R_C}\end{bmatrix}\Delta d \tag{2.24}$$

2.6 Summary

This chapter provides general background information of boost converter and develops the complete mathematical model of the boost converter based on the averaging method. A linear model is also developed that could be used for control design using the PI method and the LQR method.

CHAPTER 3

PI CONTROL

3.1 Introduction

Presented in this chapter is the control design for DC-DC boost converter using linear control methods. For linear controller design, we use small signal approximation (2.23) of the average model developed in Chapter 2. The accurate average models for boost converters were obtained using the standard state-space averaging techniques.

In this chapter, we use frequency response and root locus methods to design linear controllers. In the frequency response method, an analog PI controller is designed based on the small signal model (2.23). The system is compensated to achieve high loop gain, wide bandwidth and sufficient phase margin.

3.2 PI Controller Design

The PI controller is designed based on the linearized model developed in Chapter 2. The transfer function of the open loop circuit from linearized system between the input duty cycle ΔD and the output voltage ΔV_O is computed as:

$$G = \frac{-2199s + 4.877e^5}{s^2 + 82.51s + 1.605e^4} \tag{3.1}$$

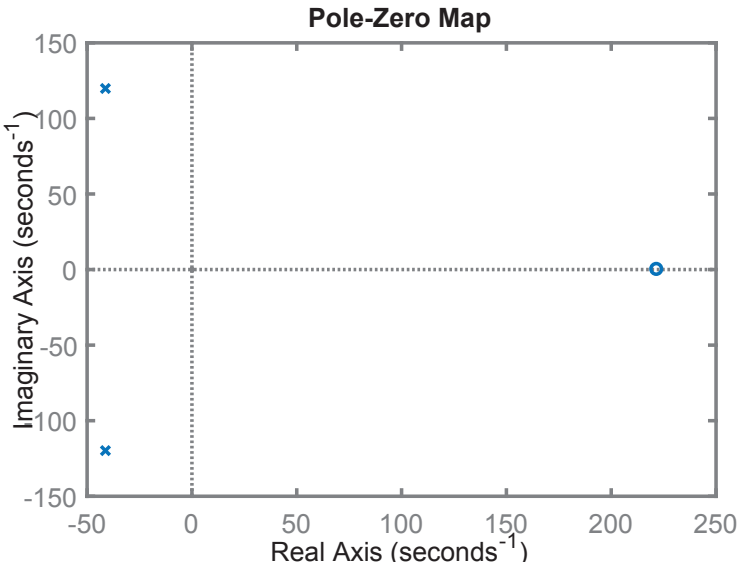

Figure 3.1: Pole and Zero Map of Linearized System

As can be seen in Fig. 3.1, the system has a large zero at $s = 291$ which leads to a big overshoot. And this is a non-minimum phase system so high gain control can not be used, because high gain will make the close loop system to become unstable. The control goal of the system is addressed on two aspects: first on tracking the desired output voltage by controlling the duty cycle and secondly for rejecting the load disturbance. Since high gain control is not applied, the integral control is necessary so as to eliminate any steady state error.

Using Ziegler-Nichols tunning method, the PI controller is designed as:

$$G_c(s) = 0.01 + \frac{1.2}{s} \tag{3.2}$$

Then the root locus and bode plot of close loop are shown in Fig. 3.2 and Fig. 3.3, respectively. Since a gain and an integration element are added in the system, the controller zero at the origin and the pole close to the origin can make the

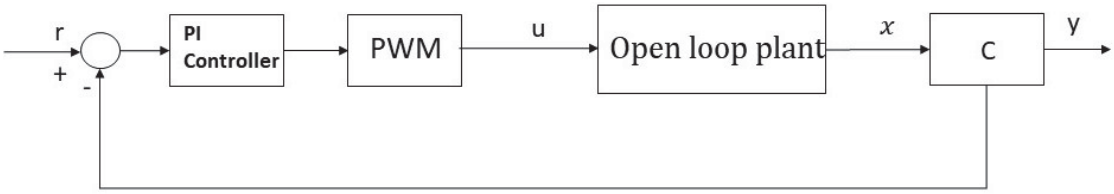

Figure 3.4: PI Controller Close Loop Diagram

stable and track the reference without error. For the closed loop system, the phase margin is about 101 deg and the gain margin is about 52db.

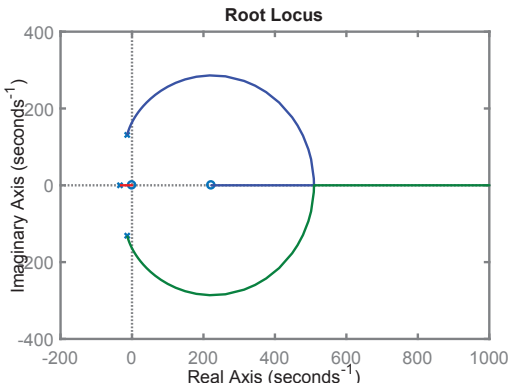

Figure 3.2: Root Locus Plot

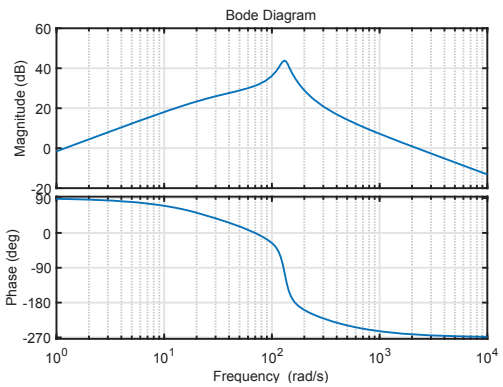

Figure 3.3: Bode Plot

3.3 Simulation Results

With the boost converter model linearized around a series of operating points and controllers developed in last section, simulation results are presented in this section. The boost converter with closed loop PI controller action is simulated in Matlab/Simulink. Boost converter Simulink schematic is shown in Fig. 3.5 and the output voltage response is shown in Fig. 3.6 Fig. 3.6 shows that the system with PI controller quickly settles to the desired steady state value 12

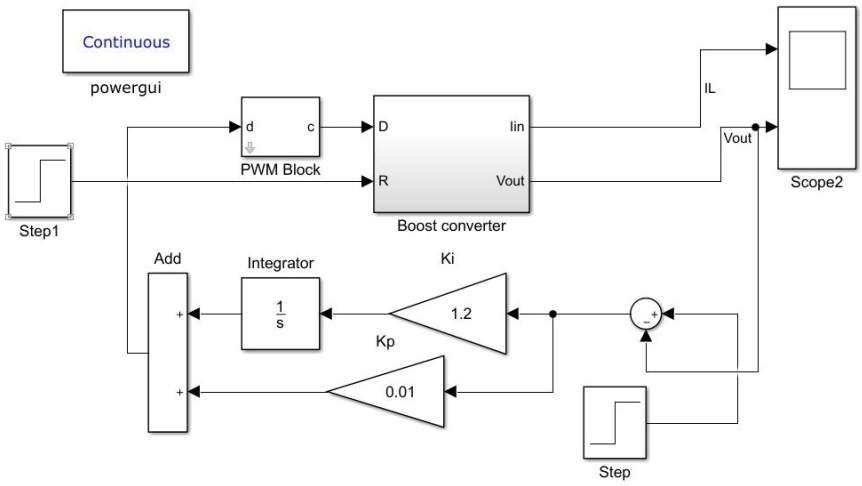

Figure 3.5: Boost Converter Matlab/Simulink Schematic

volts. The settling time is 0.251s and the overshoot is 0.22 volts, which verify the PI controller works on the system. Fig. 3.7 shows the close loop response under load disturbance; the load changed from 13Ω to 6.5Ω at 0.5s. Clearly, we can observe the inductor current and the load voltage quickly settled to steady state values after the disturbance is applied.

3.4 Controller Performance due to Reference Variation

In some practical scenarios, the reference set point may be varied to meet the output demand. For example, in power grid, depending on electric usage by end-use customers, load voltage changes with variations in load. Although the control method of power grid is much more complicated than that of this thesis, it is still worth to investigate the performance of the PI controller under varying reference set point.

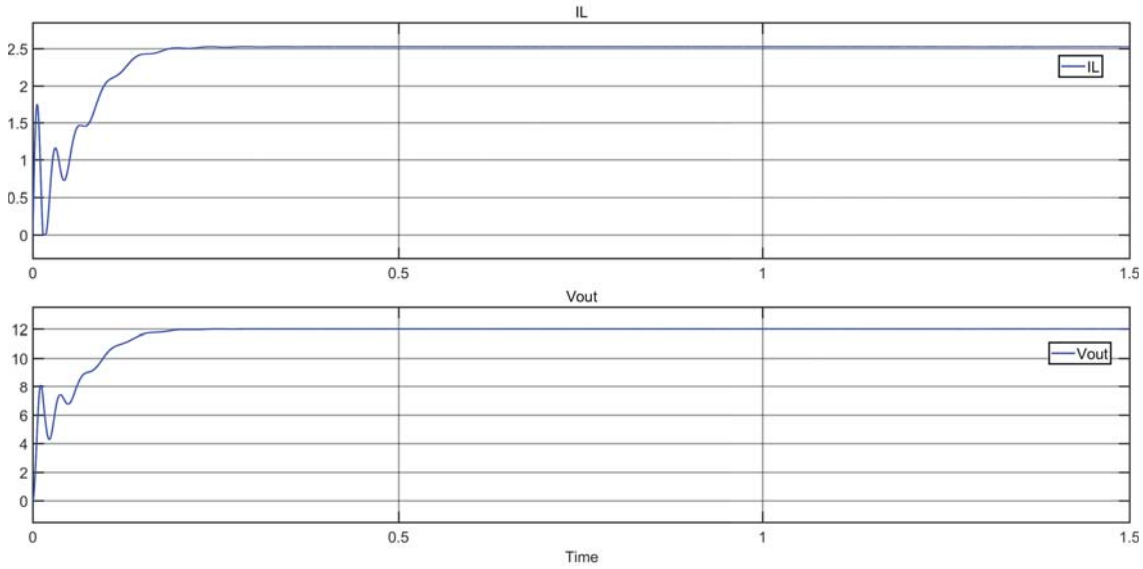

Figure 3.6: Simulation of The PI Controller

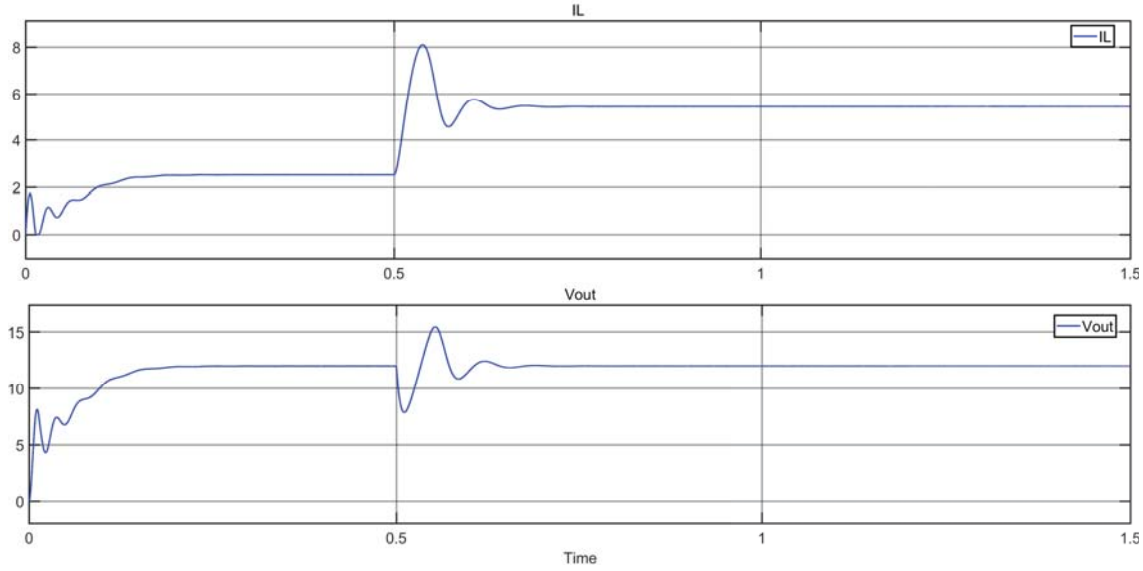

Figure 3.7: Simulation of The PI Controller in Load Disturbance

In this section, we simulate and evaluate the performance of PI controller designed above under several different references. All parameters are stay identical as before; also a load disturbance is added at $t = 0.5s$. Simulations results for several set point variaitons are shown below: From the Fig. 3.8, this PI

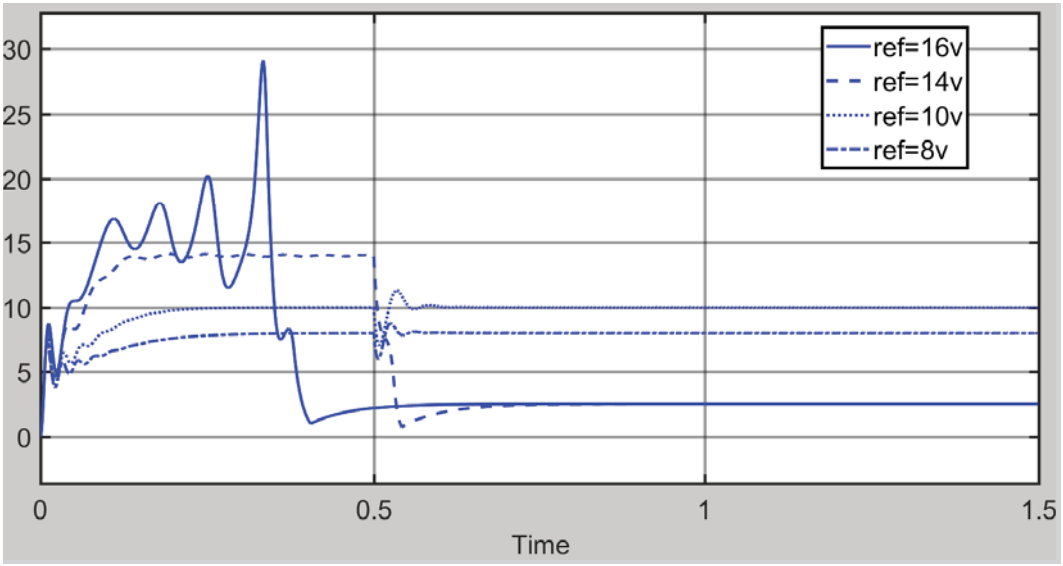

Figure 3.8: Performance of Reference Variation

controller works under 8v and 10v reference although they have longer setting time. However, for 14v and 16v reference, the output voltage can not approach expected reference value and the inductor's current is extremely high. It is also worth noting here that the average model was linearized for 12V output voltage. Based on simulation results, it is clear that the performance of the converter is not acceptable for large variations in the reference voltage. For this issue, other method such as nonlinear control should be considered.

3.5 Summary

This chapter shows a PI control method for the boost converter. The simulations have been done by Matlab/Simulink software. The PI controller works as intended, as the output voltage can approach the expected value. Furthermore, performance and robustness are tested by load variations and set point variations. The PI controller as design is acceptable if the system state is closed to the operating point.

CHAPTER 4

LQR CONTROL

4.1 Introduction

This chapter considers optimal control problem of minimizing the mean deviation of the output voltage of the boost converter with respect to the nominal set point. The theory of optimal control is concerned with operating a dynamic system at minimum cost where the system dynamics are described by a set of linear differential equations and the cost is described by a quadratic function commonly known as Linear Quadratic Control problem [20]. One of the main results in the theory is that the solution is provided as a feedback controller, which is ideal for practical implementation. It is a well-known method that provides optimally controlled feedback gains to enable the closed-loop stable with high performance.

4.2 Control Design: LQR

For infinite-time horizon, consider the continuous linear system equation (2.23) described in Chapter 2 which is rewritten below for quick reference:

$$\begin{bmatrix} \Delta\dot{x_1} \\ \Delta\dot{x_2} \end{bmatrix} = \begin{bmatrix} -\frac{RR_C}{L(R+R_C)}(1-d) - \frac{R_L}{L} & -\frac{R}{L(R+R_C)}(1-d) \\ \frac{R}{C(R+R_C)}(1-d) & -\frac{1}{C(R+R_C)} \end{bmatrix} \begin{bmatrix} \Delta x_1 \\ \Delta x_2 \end{bmatrix} + \begin{bmatrix} \frac{R(R_C I_{ss}+V_{ss})}{L(R+R_C)} \\ -\frac{RI_{ss}}{C(R+R_C)} \end{bmatrix} \Delta d \tag{4.1}$$

The LQR problem is defined as follows: find the control input u, that makes the following cost function as small as possible,

$$J = \lim_{T\to\infty} \frac{1}{T} \int_0^T (x'Qx + u'Ru)dt \tag{4.2}$$

where $(')$ stands for transpose. Here Q and R are denoted as positive definite weighting matrices which set the importance of state feedback and controller outputs, respectively. Note that $x'Qx$ is the energy of the controlled output and $u'Ru$ is the energy of the control signal. The LQR control schematic with a standard negative feedback loop is shown in fig. 4.1,

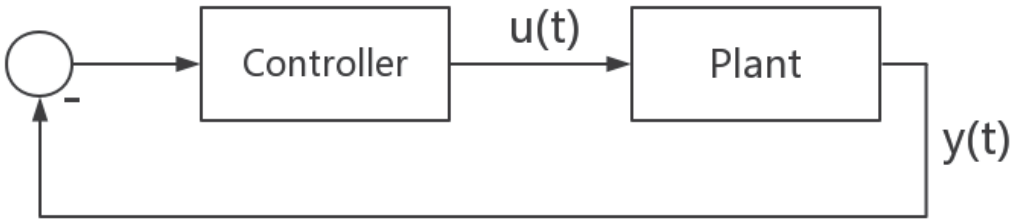

Figure 4.1: Block Diagram of LQR Control

The optimal control law is given as $u = -Kx$ where $K = R^{-1}BP$ and P is the solution to the steady state Riccati equation:

$$A'P + PA - (PB)R^{-1}(B'P) + Q = 0 \tag{4.3}$$

For tracking the reference and providing zero steady state error, an integral feedback is required as shown below:

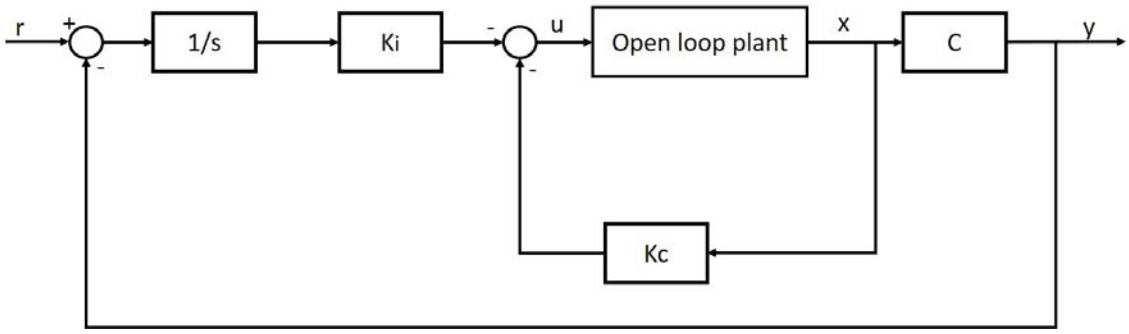

Figure 4.2: LQR Control with Integrator

The system model is augmented by defining a new state z as given in the following equation:

$$\begin{bmatrix} \dot{x} \\ \dot{z} \end{bmatrix} = \begin{bmatrix} A & 0 \\ -C & 0 \end{bmatrix} \begin{bmatrix} x \\ z \end{bmatrix} + \begin{bmatrix} B \\ 0 \end{bmatrix} u + \begin{bmatrix} 0 \\ 1 \end{bmatrix} r$$

$$y = \begin{bmatrix} C & 0 \end{bmatrix} \begin{bmatrix} x \\ z \end{bmatrix}$$

Given the augmented system, a state space controller is designed as:

$$u = -K_c x - K_i z$$

where the controller gains K_c and K_z are computed using standard LQR tools in Matlab.

4.3 Simulation Results

In this section, simulation results are presented for the LQR controller. The circuit parameters are identical as presented in Chapter 2. The reference output voltage is $V_o = 12V$. We select the matrices Q and R by balancing the relative importance of the control effort u and state error (deviation from 0), respectively. Since we focus on tracking the desired signal, different selection of the last element of Q matrix are chosen as:

$$Q_1 = \begin{bmatrix} 1 & 0 & 0 \\ 0 & 1 & 0 \\ 0 & 0 & 100 \end{bmatrix}, \quad Q_2 = \begin{bmatrix} 1 & 0 & 0 \\ 0 & 1 & 0 \\ 0 & 0 & 1000 \end{bmatrix}, \quad Q_3 = \begin{bmatrix} 1 & 0 & 0 \\ 0 & 1 & 0 \\ 0 & 0 & 10000 \end{bmatrix}, \quad R = 1$$

The optimal controller is found according to the equation (4.3) as:

$$\begin{aligned} K_1 &= [2.30 \quad 0.24 \quad -10] \\ K_2 &= [7.83 \quad 1.23 \quad -98] \\ K_3 &= [9.72 \quad 2.42 \quad -316.23] \end{aligned} \tag{4.4}$$

Fig. 4.3 shows all states via LQR controller which shows that the controller works as expected since all states approach the zero state within $0.05s$. As expected, all states, which represent a small increment, should go to zero state after an initial state error is applied. It implies that the original states will track the nominal value.

A Matlab/simulink simulation is also used to verify the controller performance for load variation for different Q matrices. The load voltage returned to the desired set point 12V very quickly and without oscillations. Fig. 4.4 shows the output voltage performance with same load disturbance(changed from 13Ω to 7.5Ω at 0.5s), respectively. Clearly, the system states can track the nominal value within a short time and reject load disturbance as well.

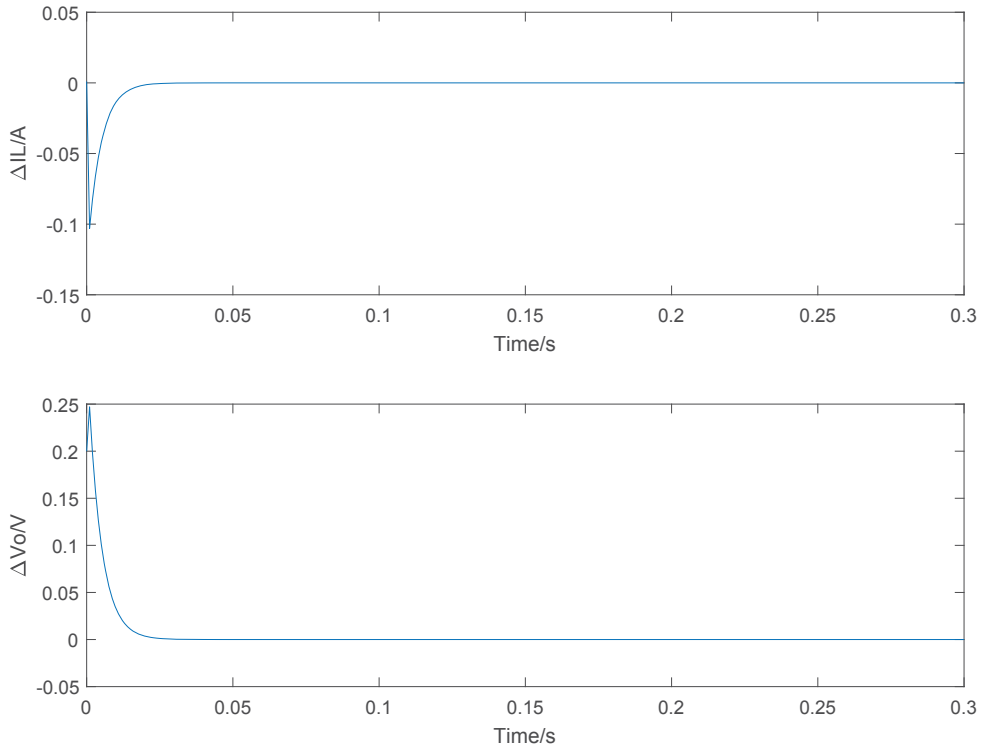

Figure 4.3: Boost Converter with LQR Controller

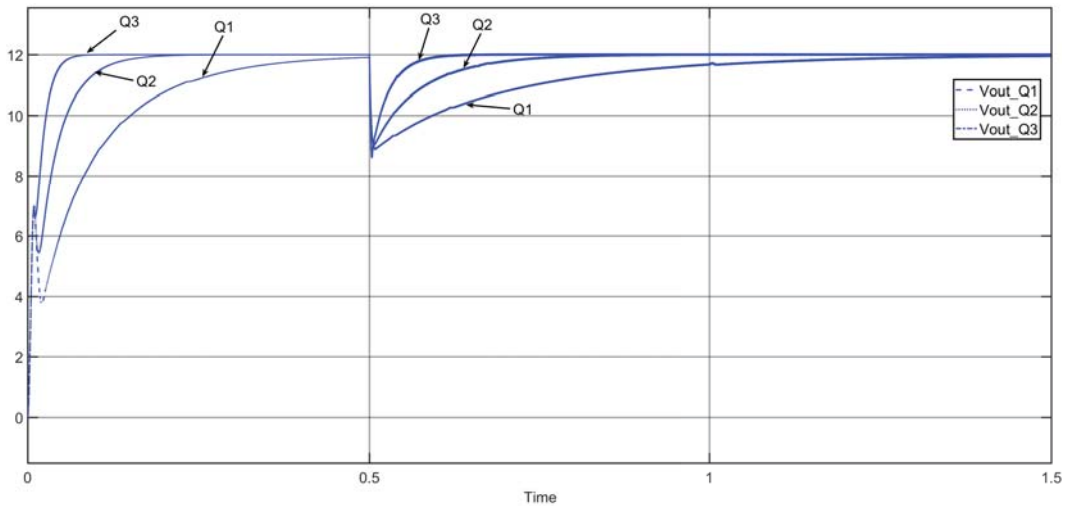

Figure 4.4: Boost Converter LQR Controller in Load Disturbance

The response of LQR controller is also compared with the PI controller as shown in fig. 4.3. We can easily see that the LQR response are much better than the PI response. Comparing the controllers in Table (4.1), we observe that both PI and LQR controllers have zero steady state error, however the LQR has a faster settling time of 0.05s while the PI controller has a larger settling time of 0.41s. However, for the overshoot index, when load disturbance occurs, PI controller has a significant overshoot.

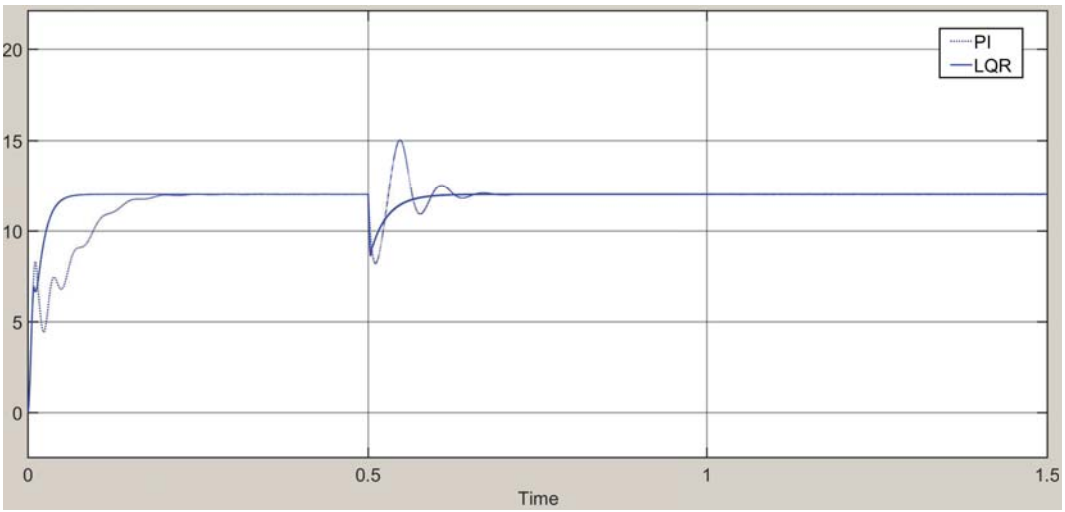

Figure 4.5: Comparison Between PI and LQR Controller

Table 4.1: Summary of Performance Index for Output Voltage

Response index	PI	LQR
Settling Time (T_S)	$0.41s$	$0.05s$
Percent Overshoot	25.0%	0.0%
Steady Stae Error	0	0

Regarding real implementation, which controller should be applied depends on application. For example, in a power system, the key for a device is to recover from faults. So if the overshoot is in a acceptable range, a faster response time controller is a better choice.

4.4 LQR Controller for Reference Variation

In section 3.5, we have evaluated the performance of PI controller under different reference set pointa. Similarly, in this section, for LQR controller is evaluated under 8V, 10V, 14V and 16V reference set points. The result is shown in Fig. 4.6.

As observed from the figure, the LQR controller works well under 8v and 10v references as in PI controller. However for 14v and 16v references, although the output voltage can approach the desired signal in the beginning, it can not reject load disturbance at 0.5s. This is also a significant drawback of the controller for using more advanced control concepts.

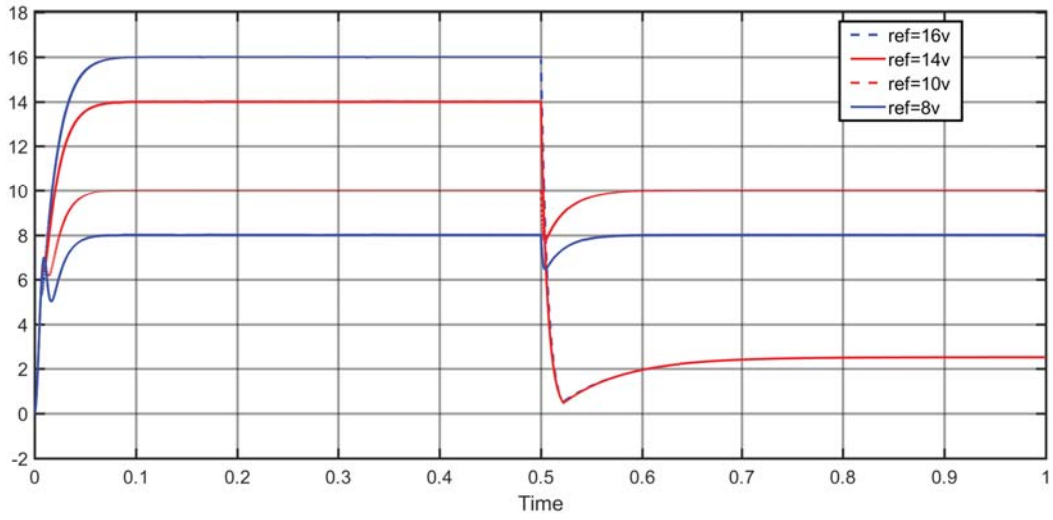

Figure 4.6: LQR Performance of Reference Variation

4.5 Summary

In this chapter, a LQR controller for the boost converter is successfully designed. The LQR problem definition and solution is summarized and the solution is applied to the linearized boost converter model presented in Chapter 2. The response of the system is plotted via Matlab code and Simulink. For the gains as chosen in this research, the LQR shows a better performance compared with the PI controller.

CHAPTER 5

NONLINEAR CONTROL

5.1 Introduction

In Chapters 3 and 4, we discussed control of boost converters using PI and LQR methods which are based on analyzing the linearized approximated system (small signal model) to find control law. However, the control law from analysis of linear approximated model only guarantees the stability with respect to the operating point of state and input variables with small perturbations. As seen in previous chapters, it is difficult to stabilize the system under large perturbations.

This chapter presents a stabilizing control method for boost converter described by a discrete time bilinear model. As introduced in Chapter 2, the state space averaging model of the boost converter is represented by a set of bilinear differential equations [21]. In general, stability analysis and output regulation problem of bilinear systems are significantly more complicated than that for linear systems. This chapter uses nonlinear control concepts [22] for output regulation of boost converters without using any linearization.

5.2 Control Design

As discussed in Chapter 2, the bilinear state space averaging model of the boost converter is given by:

$$\begin{bmatrix} \dot{x_1} \\ \dot{x_2} \end{bmatrix} = \begin{bmatrix} -\frac{RR_C}{L(R+R_C)}(1-d) - \frac{R_L}{L} & -\frac{R}{L(R+R_C)}(1-d) \\ \frac{R}{C(R+R_C)}(1-d) & -\frac{1}{C(R+R_C)} \end{bmatrix} \begin{bmatrix} x_1 \\ x_2 \end{bmatrix} + \begin{bmatrix} -\frac{V_D}{L}(1-d) + \frac{V_{in}}{L} \\ 0 \end{bmatrix} \tag{5.1}$$

$$y = \begin{bmatrix} \frac{RR_C}{R+R_C}(1-d) & \frac{R}{R+R_C} \end{bmatrix} \begin{bmatrix} x_1 \\ x_2 \end{bmatrix} \tag{5.2}$$

Equation (5.1) can be symbolically rewritten as:

$$\dot{x} = A_c x + u M_c x + g_c \tag{5.3}$$

where input variable u is duty cycle d in equation (5.1) and the matrices A_c, M_c, and g_c are as follows:

$$\begin{aligned} A_c &= \begin{bmatrix} -\frac{RR_C}{L(R+R_C)} - \frac{R_L}{L} & -\frac{R}{L(R+R_C)} \\ \frac{R}{C(R+R_C)} & -\frac{1}{C(R+R_C)} \end{bmatrix} \\ M_c &= \begin{bmatrix} \frac{RR_C}{L(R+R_C)} & \frac{R}{L(R+R_C)} \\ -\frac{R}{C(R+R_C)} & 0 \end{bmatrix} \\ g_c &= \begin{bmatrix} \frac{V_{in}}{L} \\ 0 \end{bmatrix} \end{aligned} \tag{5.4}$$

For designing the nonlinear controller, equation (5.3) is converted to a discrete time single input bilinear system described by:

$$x_{k+1} = Ax_k + u_k M x_k + G \tag{5.5}$$

$$y = cx_k \tag{5.6}$$

where input variable u is duty cycle d in equation (5.1) and A, M, G, c are as follows:

$$A = e^{A_c T} = \begin{bmatrix} 0.9409 & -0.1047 \\ 0.9420 & 0.8738 \end{bmatrix} \tag{5.7}$$

$$M = \int_0^T e^{A_c t} M_c \, dt = \begin{bmatrix} 0.0537 & 0.1088 \\ -0.9447 & 0.0536 \end{bmatrix} \tag{5.8}$$

$$G = \int_0^T e^{A_c t} g_c \, dt = \begin{bmatrix} 0.5440 \\ 0.2678 \end{bmatrix} \tag{5.9}$$

$$c = \begin{bmatrix} 0 & 1 \end{bmatrix} \tag{5.10}$$

$$x_k = \begin{bmatrix} x_{1k} \\ x_{2k} \end{bmatrix} = \begin{bmatrix} i_L \\ v_o \end{bmatrix}_k \tag{5.11}$$

The sampling time $T = 0.001$ is determined by eigenvalues of the system. The control goal is to design a control law u_k making the output v_o tracks the reference y^* without using any linearizaiton. In normal operation, the bilinear system satisfies the following equation from equation (5.5):

$$Ax^* + u^* M x^* + G = 0 \tag{5.12}$$

where x^* and u^* are state and input variables, respectively, when the system is in normal operation. Note that x_2^* can be considered as reference y^* so that we can find the reference input u^*.

Define:

$$\hat{x}_k = x_k - x^* \tag{5.13}$$

$$\hat{u}_k = u_k - u^* \tag{5.14}$$

Substitute the above equations in equation (5.5)

$$\hat{x}_{k+1} = A(\hat{x}_k + x^*) + (\hat{u}_k + u^*)M(\hat{x}_k + x^*) + G \tag{5.15}$$

By equation (5.12), the above equation is simplified to

$$\hat{x}_{k+1} = (A + u^* M)\hat{x}_k + (Mx^*)\hat{u}_k + \hat{u}_k M\hat{x}_k \tag{5.16}$$

which we denote as

$$\hat{x}_{k+1} = \hat{A}\hat{x}_k + \hat{B}\hat{u}_k + \hat{u}_k M\hat{x}_k \tag{5.17}$$

To design the controller, the objective now is to find a proper $\hat{u}_k$ so that $\hat{x}_k$ is 0. For the control design, we use the Lyapunov method as discussed in [23] and [24].

A Lyapunov function candidate for driving the control law is selected as:

$$V(\hat{x}_k) = \hat{x}_k' P\hat{x}_k \tag{5.18}$$

where P is a unique real symmetric positive-definite matrix satisfying the following discrete Lyapunov equation:

$$(1+\gamma)\hat{A}' P\hat{A} - P + I_n = 0 \tag{5.19}$$

where γ is a positive constant satisfying

$$\sqrt{1+\gamma}\, r(\hat{A}) < 1 \tag{5.20}$$

and $r(\hat{A})$ means spectral radius of matrix $\hat{A}$. It is also assumed that the original uncontrolled system is stable so that $r(\hat{A}) < 1$. Note that for the boost converter circuit considered here, this condition is always satisfied.

Following [23], the nonlinear feedback control law can be derived as:

$$\hat{u}_k = \frac{-\kappa K\hat{x}_k}{\sqrt{1 + \hat{x}_k' K' K\hat{x}_k}} \tag{5.21}$$

where the matrix K can be designed using $\hat{A}$ and $\hat{B}$ by LQR method discussed in chapter 4 and κ satisfies the inequality:

$$\kappa < \kappa^* = \frac{1}{\sqrt{2}} \min\Big\{ \Big(\frac{\gamma}{(1+\gamma)^2 ||K'\hat{B}' P\hat{B}K||}\Big)^{\frac{1}{2}}, \Big(\frac{\gamma^2}{(1+\gamma)^2 ||M'PM||}\Big)^{\frac{1}{2}} \Big\} \tag{5.22}$$

The control law defined in equation (5.21) guarantees globally asymptotically stable equilibrium point of equation (5.17) which was proved in [23] and [24].

Before discussing proof of equation(5.21), an important lemma which was proposed in [25] has to be reviewed.

Lemma 1 *Consider the matrices A, B and C, which have the same dimensions, and $C = A+B$. Then for any positive constant γ and positive definite symmetric matrix D, the following relation holds:*

$$CDC' \leq (1+\gamma)ADA' + (1+\gamma^{-1})BDB' \tag{5.23}$$

The proof of control law (5.21) is shown below:

Proof:

The close loop system (5.17) can be rewritten using the control law (5.21) as:

$$\hat{x}_{k+1} = (\hat{A} - \frac{\kappa\hat{B}K}{\sqrt{1+\hat{x}_k'K'K\hat{x}_k}} - \frac{\kappa M\hat{x}_k K}{\sqrt{1+\hat{x}_k'K'K\hat{x}_k}})\hat{x}_k \tag{5.24}$$

For notational simplicity, we shall denote $\varphi = 1 + \hat{x}_k'K'K\hat{x}_k$. Denoting $\Delta V \triangleq \Delta V(x_k) = \hat{x}_{k+1}'P\hat{x}_{k+1} - \hat{x}_k'P\hat{x}_k$ and using the above equation, the Lyapunov forward difference is derived as:

$$\Delta V = \hat{x}_k'(\hat{A} - \frac{\kappa}{\sqrt{\varphi}}(\hat{B}K + M\hat{x}_k K))'P(\hat{A} - \frac{\kappa}{\sqrt{\varphi}}(\hat{B}K + M\hat{x}_k K))\hat{x}_k - \hat{x}_k'P\hat{x}_k \tag{5.25}$$

Using Lemma 1 and (5.19), equation (5.25) can be rewritten as:

$$\Delta V \leq \hat{x}_k'(-I_n + \frac{\kappa^2}{\varphi}\frac{(1+\gamma)^2}{\gamma}K'\hat{B}'P\hat{B}K + \frac{\kappa^2 K'\hat{x}_k'\hat{x}_k K}{\varphi}\frac{(1+\gamma)^2}{\gamma^2}M'PM)\hat{x}_k \tag{5.26}$$

Since for any x_k and K the following inequalities are always satisfied:

$$\frac{K'\hat{x}_k'\hat{x}_k K}{1+\hat{x}_k'K'K\hat{x}_k} \leq 1 \tag{5.27}$$

$$\frac{1}{1+\hat{x}_k'K'K\hat{x}_k} \leq 1 \tag{5.28}$$

So equation (5.26) can be simplified as :

$$\Delta V \leq \hat{x}_k'(\frac{2(1+\gamma)^2}{\gamma}\max\{||K'\hat{B}'P\hat{B}K||, \frac{1}{\gamma}||M'PM||\}\kappa^2 I_n - I_n)\hat{x}_k \tag{5.29}$$

Clearly the right hand side of (5.48) is negative definite if and only if:

$$\max\{||K'\hat{B}'P\hat{B}K||, \frac{1}{\gamma}||M'PM||\}\kappa^2 < \frac{\gamma}{2(1+\gamma)^2} \tag{5.30}$$

The above inequality verifies (5.22) so completes the control algorithm.

Combining equations (5.43), (5.44) and (5.21), we obtain the feedback law:

$$u_k = u^* - \frac{\kappa K(x_k - x^*)}{\sqrt{1 + (x_k - x^*)'K'K(x_k - x^*)}} \tag{5.31}$$

Using the control law equation (5.31), the bilinear system equation (5.5) can be controlled.

5.3 Simulation Results

In this section, the proposed control algorithm is applied to the boost converter. Fig. 5.1 shows the nonlinear control diagram. The circuit parameters are identical as described in chapter 3 and 4. The reference voltage is $V_o = 12V$. Parameters γ and κ are selected as 0.1 and 0.0084, respectively. Matrices P and K are computed as:

$$P = \begin{bmatrix} 396.35 & -29.07 \\ -29.07 & 41.11 \end{bmatrix} \tag{5.32}$$

$$K = \begin{bmatrix} 0.76 & 0.02 \end{bmatrix} \tag{5.33}$$

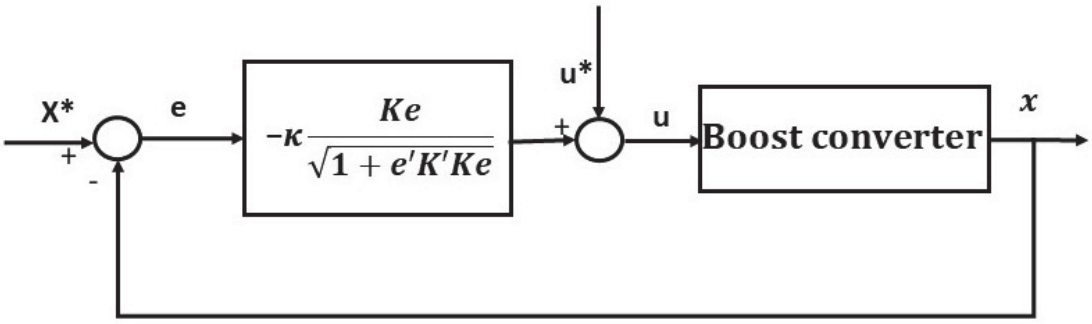

Figure 5.1: Nonlinear Control Close-loop Diagram

5.3.1 Step Change in Load

Fig. 5.2 shows the trajectories of states and inputs for tracking reference under a step change of load resistance. The load varied from 13Ω to 6.5Ω at 0.5s. Clearly, we can observe that the nonlinear controller has good voltage tracking performance and there is no excessive inductor input current.

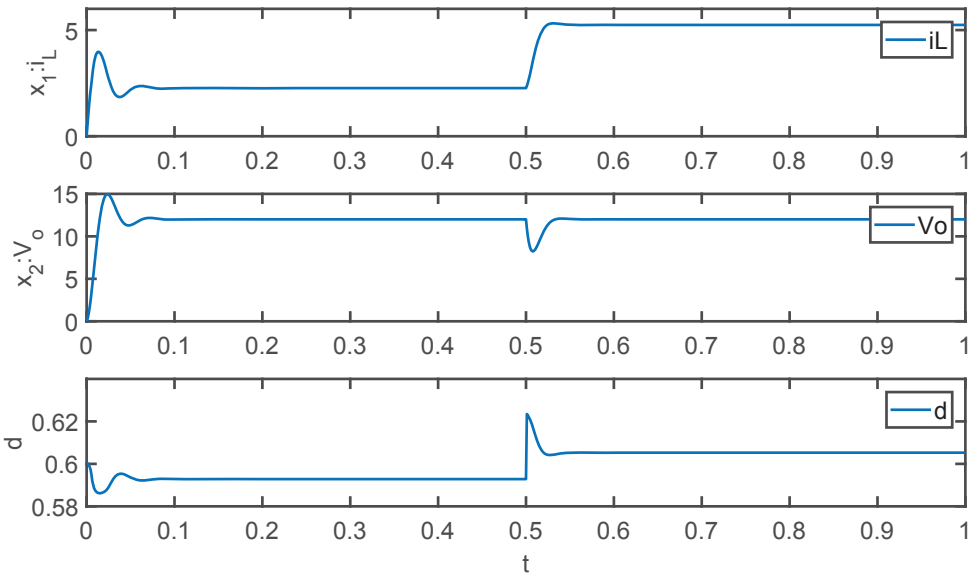

Figure 5.2: Boost Converter with Nonlinear Controller in Load Disturbance

5.3.2 Load Pulse

Fig. 5.3 presents the performance of the system under load pulse. The load changes from 13Ω to 6.5Ω at 0.5s then increases to 19.5Ω at 0.55s and goes back to 13Ω at 0.6s. It shows that the boost converter with nonlinear controller is able to reject the load pulse and all states settle down to expected values, which verifies the robust stability in wide range variation of load resistance.

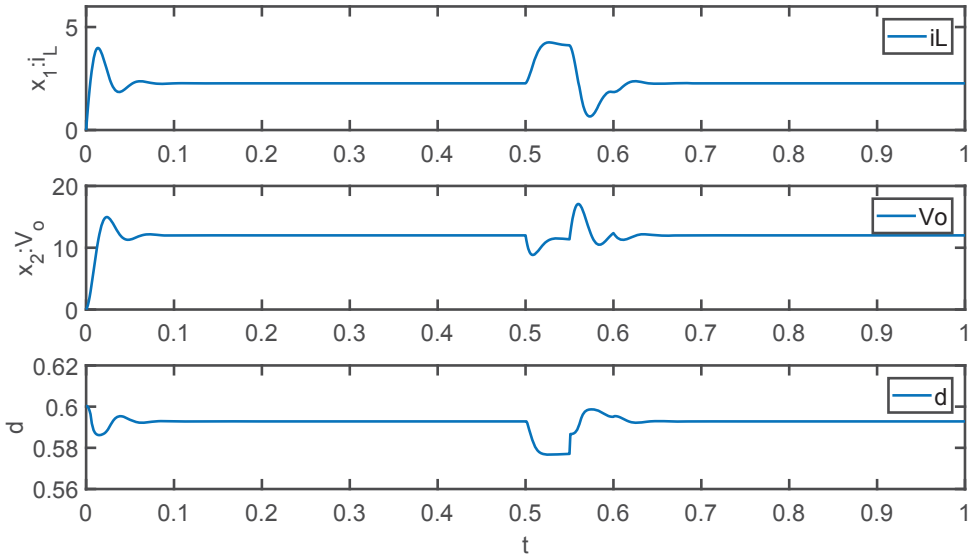

Figure 5.3: Boost Converter with Nonlinear Controller in Load Pulse

5.3.3 Change in Reference

Next we investigate the closed loop performance for variations of reference set point. Fig. 5.4, 5.5 and 5.6 show that the system converges to desired point under different references. Also along with the change of reference set point, we apply changes in load resistance. Comparing with Fig. 4.4 and 3.8, we observe that not only can the boost converter with nonlinear controller approach to different

desired reference but also be stabilized under load pulse.

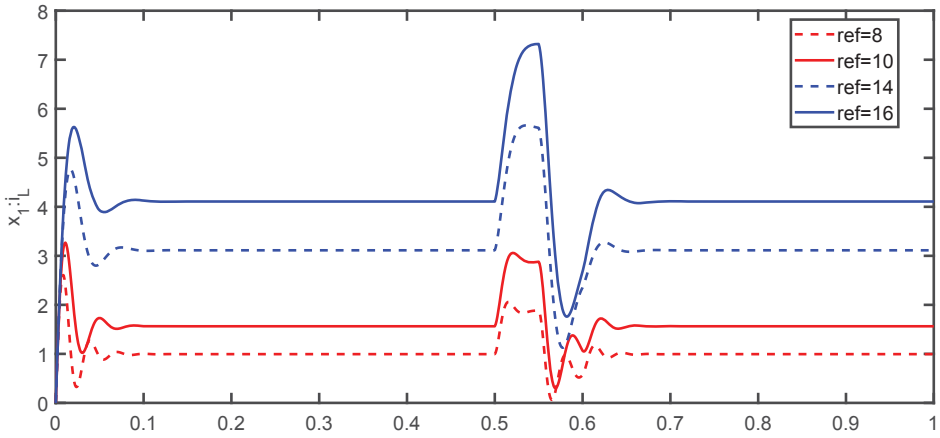

Figure 5.4: Input Current for Different Reference

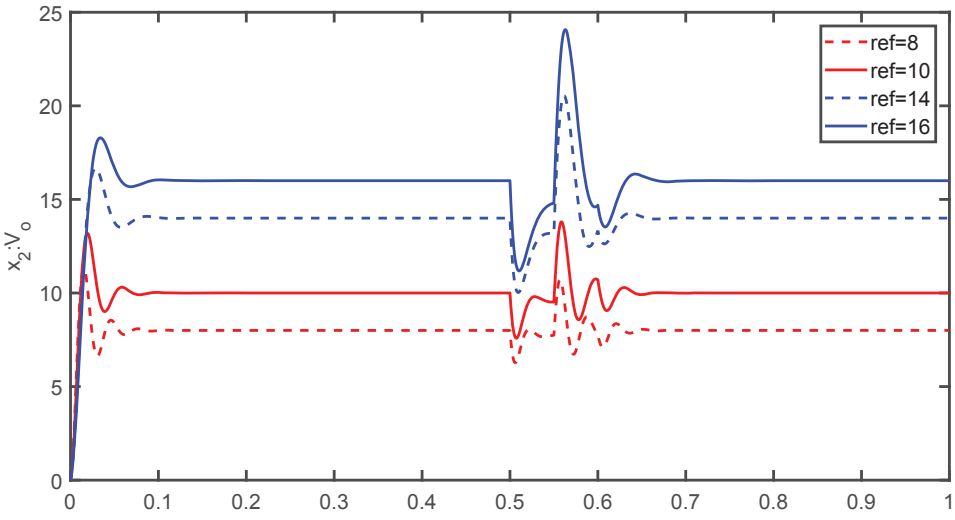

Figure 5.5: Output Voltage for Different Reference

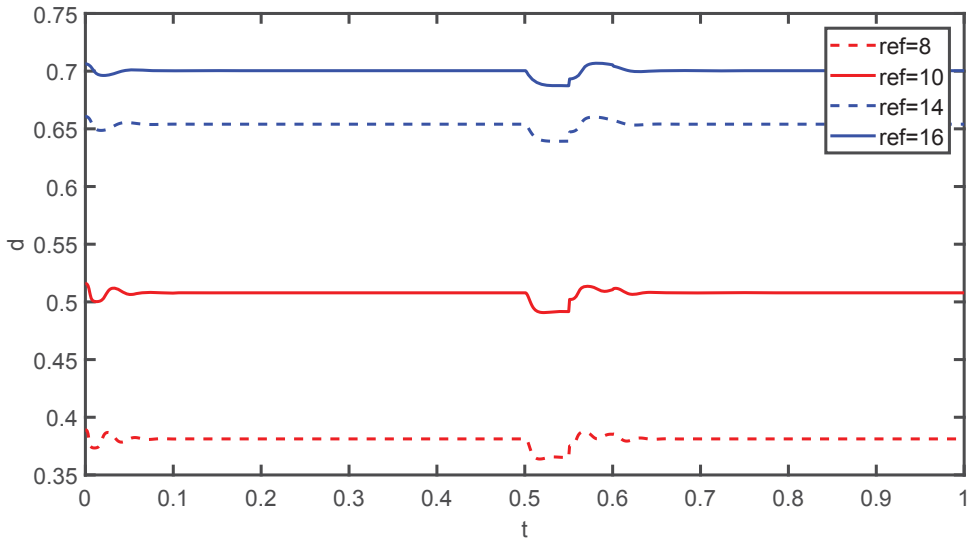

Figure 5.6: Duty Cycle for Different Reference

5.4 Gaussian Disturbance of Load

In real applications, loads are not just varied in steps or in any regular way, rather loads can change randomly. For example, in power systems, load variations are common due to temporary short circuits along transmission lines, additional sources of friction that appear momentarily in generators and motors, and varying electrical loads downstream. This section considers the boost converter performance under a stochastic resistive load.

5.4.1 System Modeling and Control Design

For modeling the controller, it is assumed that the load resistance varies as $R + \Delta R$, where ΔR is a zero mean Gaussian distributed random process representing random variations of the load. The system model matrices given

in equation (5.4) are then modified as:

$$A_c = \begin{bmatrix} -\frac{(R+\Delta R)R_C}{L((R+\Delta R)+R_C)} - \frac{R_L}{L} & -\frac{(R+\Delta R)}{L((R+\Delta R)+R_C)} \\ \frac{(R+\Delta R)}{C((R+\Delta R)+R_C)} & -\frac{1}{C((R+\Delta R)+R_C)} \end{bmatrix} \tag{5.34}$$

$$M_c = \begin{bmatrix} \frac{(R+\Delta R)R_C}{L((R+\Delta R)+R_C)} & \frac{(R+\Delta R)}{L((R+\Delta R)+R_C)} \\ -\frac{(R+\Delta R)}{C((R+\Delta R)+R_C)} & 0 \end{bmatrix} \tag{5.35}$$

For the convenience of computation and design, only first order variation of the above matrices are considered. Then it is verified that for small variations of ΔR, we have

$$A_c = \begin{bmatrix} -\frac{RR_C}{L(R+R_C)} - \frac{R_L}{L} & -\frac{R}{L(R+R_C)} \\ \frac{R}{C(R+R_C)} & -\frac{1}{C(R+R_C)} \end{bmatrix} + \begin{bmatrix} 0 & 0 \\ 0 & \frac{1}{C(R+R_C)^2} \end{bmatrix} \Delta R \tag{5.36}$$

$$M_c = \begin{bmatrix} \frac{RR_C}{L(R+R_C)} & \frac{R}{L(R+R_C)} \\ -\frac{R}{C(R+R_C)} & 0 \end{bmatrix} \tag{5.37}$$

This gives us the stochastic model of the boost converter under random load variations as:

$$\dot{x} = A_c x + u M_c x + E_c x\,\eta + g_c \tag{5.38}$$

where

$$E_c = \begin{bmatrix} 0 & 0 \\ 0 & \frac{1}{C(R+R_C)^2} \end{bmatrix} \tag{5.39}$$

and $\eta(t) = \Delta R$ is the zero mean Gaussian process representing the random load variations. Rest of the matrices in (5.38) are same as those defined earlier.

The converter model given above is then converted to the corresponding discrete time model which is given by

$$x_{k+1} = Ax_k + u_k M x_k + Ex\,\eta + G \tag{5.40}$$

$$y = cx_k \tag{5.41}$$

with

$$E = \int_0^T e^{A_c t} E_c\, dt \tag{5.42}$$

For control design, we consider the operating point x^* and define small variations as

$$\hat{x}_k = x_k - x^* \tag{5.43}$$

$$\hat{u}_k = u_k - u^* \tag{5.44}$$

Then as shown in the previous section, from equation (5.40), the state deviation $\hat{x}_{k+1}$ satisfies:

$$\hat{x}_{k+1} = \hat{A}\hat{x}_k + \hat{B}\hat{u}_k + \hat{u}_k M\hat{x}_k + E\hat{x}_k\eta \tag{5.45}$$

We also use the same control law as in the previous section:

$$\hat{u}_k = \frac{-\kappa K\hat{x}_k}{\sqrt{1+\hat{x}_k' K' K\hat{x}_k}} \tag{5.46}$$

where the matrix K is the gain matrix that can be designed using $\hat{A}$ and $\hat{B}$ by LQR or other methods. Next we prove stability of the closed loop control system for the stochastic system (5.45) with the nonlinear controller (5.46).

Proof:

Substitute (5.46) in above model equation (5.45):

$$\hat{x}_{k+1} = (\hat{A} - \frac{\kappa\hat{B}K}{\sqrt{1+\hat{x}_k' K' K\hat{x}_k}} - \frac{\kappa M\hat{x}_k K}{\sqrt{1+\hat{x}_k' K' K\hat{x}_k}})\hat{x}_k + E\hat{x}_k\eta \tag{5.47}$$

For notational simplicity, we still denote $\varphi = 1 + \hat{x}_k' K' K\hat{x}_k$.

Denoting $\Delta V \triangleq \Delta V(x_k) = \hat{x}_{k+1}' P\hat{x}_{k+1} - \hat{x}_k' P\hat{x}_k$ and using the above equation, the Lyapunov forward difference is derived as:

$$\Delta V = \hat{x}_k'(\hat{A} - \frac{\kappa}{\sqrt{\varphi}}(\hat{B}K + M\hat{x}_k K) + E\eta)' P(\hat{A} - \frac{\kappa}{\sqrt{\varphi}}(\hat{B}K + M\hat{x}_k K) + E\eta)\hat{x}_k - \hat{x}_k' P\hat{x}_k \tag{5.48}$$

Using Lemma 1 and equation (5.19), the above equation can be rewritten as:

$$\begin{aligned}\Delta V \leq & \hat{x}_k'(-I_n + \frac{\kappa^2}{\varphi}\frac{(1+\gamma)^2}{\gamma}K'\hat{B}' P\hat{B}K + \frac{\kappa^2 K'\hat{x}_k'\hat{x}_k K}{\varphi}\frac{(1+\gamma)^2}{\gamma^2}M' PM)\hat{x}_k \\ & + (\hat{x}_k' E' P\hat{x}_k + \hat{x}_k' PE\hat{x}_k)\eta + \hat{x}_k' E' E\hat{x}_k\eta^2\end{aligned} \tag{5.49}$$

Since η is zero mean Gaussian distributed random process, so we expand and take expectation of ΔV:

$$\begin{aligned} E\{\Delta V\} \leq & E\big\{\hat{x}_k'\big(-I_n + \frac{\kappa^2}{\varphi}\frac{(1+\gamma)^2}{\gamma}K'\hat{B}'P\hat{B}K + \frac{\kappa^2 K'\hat{x}_k'\hat{x}_k K}{\varphi}\frac{(1+\gamma)^2}{\gamma^2}M'PM\big)\hat{x}_k\big\} \\ & + E\big\{\hat{x}_k'E'E\hat{x}_k q\big\} \end{aligned} \tag{5.50}$$

where q is the covariance of random process η. Then we use equations (5.27) and (5.28) to further simplify the above equation:

$$\begin{aligned} E\{\Delta V\} \leq & E\{\hat{x}_k'(-I_n + \frac{\kappa^2}{\varphi}\frac{(1+\gamma)^2}{\gamma}K'\hat{B}'P\hat{B}K + \frac{\kappa^2 K'\hat{x}_k'\hat{x}_k K}{\varphi}\frac{(1+\gamma)^2}{\gamma^2}M'PM)\hat{x}_k\} \\ & + E\{\hat{x}_k'E'E\hat{x}_k q\} \\ \leq & E\big\{\hat{x}_k'(-I_n + \frac{(1+\gamma)^2}{\gamma}\kappa^2\|K'\hat{B}'P\hat{B}K\| + \frac{(1+\gamma)^2}{\gamma^2}\kappa^2\|M'PM\| \\ & + q\|E'E\|)\hat{x}_k\big\} \\ \leq & E\big\{\hat{x}_k'(\frac{2(1+\gamma)^2}{\gamma}\max\big\{\|K'\hat{B}'P\hat{B}K\|, \frac{1}{\gamma}\|M'PM\|\big\}\kappa^2 I_n \\ & - (1 - q\|E'E\|)I_n)\hat{x}_k\big\} \end{aligned} \tag{5.51}$$

For stability of the system, it is necessary that the right side of equation (5.51) is negative definite which can be satisfied if the following two conditions are satisfied:

$$1)\ \max\big\{||K'\hat{B}'P\hat{B}K||, \frac{1}{\gamma}||M'PM||\big\}\kappa^2 < \frac{\gamma}{2(1+\gamma)^2}(1 - q||E'E||) \tag{5.52}$$

$$2)\ 1 - q||E'E|| > 0 \tag{5.53}$$

Thus it is clear that for for closed loop stability of the converter under stochastic variations of load, we obtain new stability conditions that are slightly different from that for the non-stochastic loads. In particular, we have

1. The value of κ satisfying above equation is slightly smaller than that for the non-stochastic case (5.22)

2. Secondly the system is stable only if the covariance of the load disturbance is small satisfying

$$q \leq \frac{1}{||E'E||} \tag{5.54}$$

Inequality (5.54) shows that if the covariance is too large, this stochastic system with nonlinear controller will not be stable.

For implementation of the control law we use:

$$u_k = u^* - \frac{\kappa K(x_k - x^*)}{\sqrt{1 + (x_k - x^*)'K'K(x_k - x^*)}} \tag{5.55}$$

where κ satisfies the inequality:

$$\kappa < \kappa^* = \frac{1}{\sqrt{2}}(1 - q\|E'E\|) \min\Big\{(\frac{\gamma}{(1+\gamma)^2\|K'\hat{B}'P\hat{B}K\|})^{\frac{1}{2}}, (\frac{\gamma^2}{(1+\gamma)^2\|M'PM\|})^{\frac{1}{2}}\Big\} \tag{5.56}$$

5.4.2 Simulation Results

For evaluation of the closed loop performance, we use the same control law as before, and simulate the closed loop system in Matlab/Simulink. Various parameters for the circuit and the gains of the control are also considered unchanged.

Random load variations have been simulated using the random process $\eta(t)$ with zero mean and a covariance of 2.3 which was obtained using the circuit parameters used in this research. Since this is a stochastic system, the system response is expected to be stochastic as well. Thus it is necessary to find expected values of the system states which was done by taking ensemble average of system responses for 100 independent runs. Figure 5.7 shows the result:

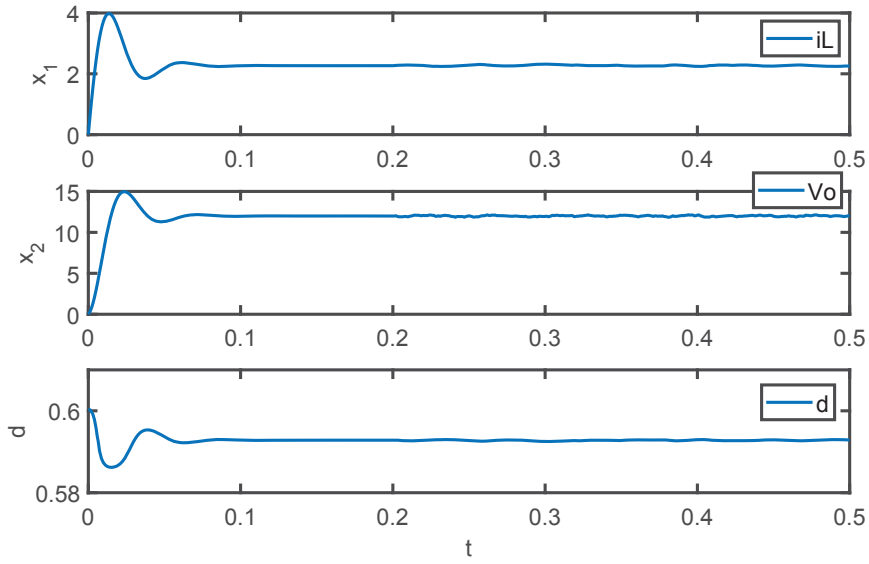

Figure 5.7: Ensemble Average of System Response for Stochastic Load

In this simulation, it was assumed that there was no changes in load resistance before 0.2s, and a random load disturbance continues from 0.2s. From fig. 5.7, it is clear that the controller can track reference voltage with small fluctuations. This simulation also verifies robust stability of the bilinear boost converter model with nonlinear controller.

5.5 Comparison with PI and LQR Controller

Comparing with PI and LQR controllers, the nonlinear control law shows a more stable and quick response under large perturbation of load resistance and different reference set points. Among these three controllers, PI controller is easy and simple to implement but has longer rise time and the LQR controller has better transient response. The nonlinear controller not only has quick response and smooth transient but also be stable under large perturbation of load resistance

and references. Even if the nonlinear controller is more complicated to implement, it is still worth to apply due to robust stability.

5.6 Summary

This chapter presents a nonlinear control algorithm based on bilinear boost converter model. Without any linearization, the stabilizing control law is derived by Lyapunov function and applied to the state space averaging model of boost converter. Performance of the closed loop system is verified by Matlab simulations for larger perturbations and different references. The system has better robustness and stability comparing with PI and LQR controllers while the control algorithm is more complicated.

CHAPTER 6

CONCLUSIONS

This chapter summarizes the results of modeling and control design boost converters. Also some suggestions for further research are presented.

6.1 Summary of Results

This research investigates both analytical design and numerical simulation work for control of a boost converter. An average model is derived from switch model of a specific DC-DC boost converter, which is proved to approximate the switch model behavior. The system model is shown to be given by a bilinear differential equation. For control design using linear control methods, the bilinear model is linearized with respect to an operating state giving rise to a linear system model.

For controlling the boost converter, three different control methods have been considered. For applying linear control concepts, we use the PI control and the LQR control. Both methods work very well under small variations with respect to the operating point. For the gains as chosen in this research, overall the LQR method performs better than the PI control because of its faster response time and no overshoot, however practical implementation of the PI control might be relatively easier. Performance of the PI control and the LQR control was relatively poor for large disturbances, such as a large change is set point.

In order to make the system stable in large perturbations, a nonlinear control algorithm is applied. The simulation results verify the nonlinear controller shows a robust stability to wide range of disturbances of load resistance as well as stable and quick response to the different reference voltage.

Stability of the closed loop system was also evaluated under random variations of the load resistance. It is shown that the system is stable only if the covariance of the load is sufficiently small satisfying a certain condition as given in Section 5.4. The results are also illustrated by Matlab simulations.

6.2 Future Research

Several interesting work have not been included in this thesis. This section presents some extensions of these areas:

1) The nonlinear control algorithm in this thesis performs well. However, it's just based on the prerequisite that matrix A is stable. Although this condition is satisfied for the boost converter, further research on more general case by the nonlinear algorithm should be considered when the A matrix is not necessarily stable.

2) The hardware implementation for both control linear and bilinear algorithms is important. Proving the developed control concepts on hardware platform would be more important for practical applications.

3) All research completed in this thesis are based on voltage mode control. Future research could include current mode control which is beneficial in several ways. For example, the current could be regulated to satisfy more sensitive requirement of the load circuit. This advantage will give more protection

of the power supply and robustness to the whole system. Of course, the architecture of current mode control, which has to include both voltage and current control, will be more complicated.

REFERENCES

[1] B. Johansson, "Dc-dc converters-dynamic model design and experimental verification," 2005.

[2] C. Albea, "Control design for electronic power converters," Ph.D. dissertation, Institut National Polytechnique de Grenoble-INPG; Universidad de Sevilla, 2010.

[3] Q. Zhang, R. Min, Q. Tong, X. Zou, Z. Liu, and A. Shen, "Sensorless predictive current controlled DC –DC converter with a self-correction differential current observer," *IEEE Transactions on Industrial Electronics*, vol. 61, no. 12, pp. 6747–6757, Dec. 2014.

[4] B. K. Bose, "Energy, environment, and advances in power electronics," *IEEE Transactions on Power Electronics*, vol. 15, no. 4, pp. 688–701, Jul. 2000.

[5] B. Kurucs, A. Peschka, P. Stumpf, I. Nagy, and I. Vajk, "State space control of quadratic boost converter using lqr and lqg approaches," in *Proc. Intl Conf 2015 Intl Aegean Conf. Electrical Machines Power Electronics (ACEMP) Optimization of Electrical Electronic Equipment (OPTIM) 2015 Intl Symp. Advanced Electromechanical Motion Systems (ELECTROMOTION)*, Sep. 2015, pp. 642–648.

[6] J. Hossain and H. R. Pota, "Power system voltage stability and models of devices," *Robust Control for Grid Voltage Stability: High Penetration of Renewable Energy*, Jan. 2014. [Online]. Available: http://dx.doi.org/10.1007/978-981-287-116-9_2

[7] R. Erickson and D. Maksimovic, *Fundamentals of Power Electronics*. Kluwer Academic Publishers, 2001.

[8] J. Zeng, W. Qiao, and L. Qu, "A single-switch lcl-resonant isolated dc-dc converter," 2013.

[9] M. Forouzesh, Y. P. Siwakoti, S. A. Gorji, F. Blaabjerg, and B. Lehman, "Step-up dc–dc converters: a comprehensive review of voltage-boosting techniques, topologies, and applications," *IEEE Transactions on Power Electronics*, vol. 32, no. 12, pp. 9143–9178, 2017.

[10] N. Mohan, T. Undeland, and W. Robbins, "Power electronics: converters, drives and applications," 2002.

[11] S. H. Ham, H. j. Choe, H. S. Lee, and B. Kang, "Improvement of power-conversion efficiency of AC-DC boost converter using 1:1 Transformer," *IEEE Transactions on Power Electronics*, vol. PP, no. 99, p. 1, 2017.

[12] A. Pressman, K. Billings, and T. Morey., *Switching Power Supply Design*. McGrawHill Professional, 2009.

[13] E. Bilbao, P. Barrade, I. Etxeberria-Otadui, A. Rufer, S. Luri, and I. Gil, "Optimal energy management strategy of an improved elevator with energy storage capacity based on dynamic programming," *IEEE Transactions on Industry Applications*, vol. 50, no. 2, pp. 1233–1244, Mar. 2014.

[14] Q. Zhou, Y. Huang, F. Zeng, and Q. S. Chen, "Dynamic analysis of DC-dc boost converter based on its nonlinear characteristics," in *Proc. IECON 2006 - 32nd Annual Conf. IEEE Industrial Electronics*, Nov. 2006, pp. 1769–1774.

[15] B. Arbetter and D. Maksimovic, "Feed-forward pulse-width modulators for switching power converters," in *Proc. th Annual IEEE Power Electronics Specialists Conf. PESC '95 Record*, vol. 1, Jun. 1995, pp. 601–607 vol.1.

[16] M. B. Camara, H. Gualous, F. Gustin, A. Berthon, and B. Dakyo, "DC/dc converter design for supercapacitor and battery power management in hybrid vehicle applications —polynomial control strategy," *IEEE Transactions on Industrial Electronics*, vol. 57, no. 2, pp. 587–597, Feb. 2010.

[17] I. Alhamrouni, W. I. Hanis, M. Salem, F. M. Albatsh, and B. Ismail, "Application of DC-dc converter for e.v battery charger using PWM technique and hybrid resonant," in *Proc. IEEE Int. Conf. Power and Energy (PECon)*, Nov. 2016, pp. 133–138.

[18] A. Kavousi, S. H. Fathi, J. MiliMonfared, and M. N. Soltani, "Application of boost converter to increase the speed range of dual-stator winding induction generator in wind power systems," *IEEE Transactions on Power Electronics*, p. 1, 2018.

[19] H. K. Khalil, "Noninear systems," *Prentice-Hall, New Jersey*, vol. 2, no. 5, pp. 5–1, 1996.

[20] Y. Meng, Q. Chen, X. Chu, and A. Rahmani, "Maneuver guidance and formation maintenance for control of leaderless space-robot teams," *IEEE Transactions on Aerospace and Electronic Systems*, 2018.

[21] R. D. Middlebrook and S. Cuk, "A general unified approach to modelling switching-converter power stages," in *Proc. IEEE Power Electronics Specialists Conf*, Jun. 1976, pp. 18–34.

[22] F. D. Tan and R. S. Ramshaw, "Instabilities of a boost converter system under large parameter variations," *IEEE Transactions on Power Electronics*, vol. 4, no. 4, pp. 442–449, Oct. 1989.

[23] J.-S. Chiou, F.-C. Kung, and T. H. S. Li, "Robust stabilization of a class of singularly perturbed discrete bilinear systems," *IEEE Transactions on Automatic Control*, vol. 45, no. 6, pp. 1187–1191, Jun. 2000.

[24] B.-S. Kim, Y.-J. Kim, M. T. Lim, and B. Kim, "Stabilizing control for discrete time multi-input bilinear systems," *15th Triennial World Congress*, 2002.

[25] T. Furukawa and E. Shimemura, "Stabilizability conditions by memory less feedback for linear systems with time-delay," *International Journal of Control*, vol. 37, no. 3, pp. 553–565, 1983. [Online]. Available: https://doi.org/10.1080/00207178308932992